Multimodal Imaging Probe for Melanoma Evaluating of PTK7 Expression by Sgc8-c Aptamer Recognition

Estefanía Sicco
University of the Republic
Amy Mónaco
University of the Republic
Marcelo Fernandez
University of the Republic
María Moreno
University of the Republic
Victoria Calzada (vcalzada@cin.edu.uy)
University of the Republic
Hugo Cerecetto
University of the Republic

Research Article

Keywords: melanoma, PTK7, aptamer, DNA

Posted Date: February 17th, 2021

DOI: https://doi.org/10.21203/rs.3.rs-200306/v1

Abstract

Melanoma is one of the most aggressive and deadly skin cancers, and although histopathological criteria are used for its prognosis, biomarkers are necessary to identify the different evolution stages. The applications of molecular imaging include the *in vivo* diagnosis of cancer with probes that recognize the tumor-biomarkers specific expression allowing external images acquisitions and evaluations of the biological process in quali-quantitative ways. Aptamers are oligonucleotides that recognize targets with high affinity and specificity presenting advantages that make them interesting molecular imaging probes. Sgc8-c (DNA-aptamer) selectively recognizes PTK7-receptor overexpressed in various types of tumors. Herein, Sgc8-c was evaluated, in two melanoma models, non-metastatic and metastatic, as molecular imaging probe for *in vivo* diagnostic. Firstly, two probes, radio- and fluorescent-probe, were *in vitro* evaluated verifying the high specific PTK7 recognition and its internalization in tumor cells by the endosomal route. Secondly, *in vivo* proof of concept was performed in animal tumor models. Likewise, they have rapid clearance from blood exhibiting excellent target (tumor)/non-target organ ratios. Furthermore, optimal biodistribution was observed 24 hours after probes-injections accumulating almost exclusively in the tumor tissue. Sgc8-c is a potential tool for their specific use in the early detection of melanoma.

Introduction

Melanoma is one of the most aggressive and deadly types of skin cancer[1,2], with an annual increase in incidence during the last decade between 15–25 per 100,000 individuals[3]. Although histopathological criteria such as tumor thickness, mitotic rate, histologic subtype and ulceration[4,5], are usually used for its prognosis, biomarkers are necessary to identify whether the primary melanoma has metastasized or even differentiate the stages of its evolution[6,7]. Malignant melanomas have been reported to have increased activity of protein tyrosine kinase 7 (PKT7)[8,9]. This membrane receptor is highly conserved in different species and is involved in signal transduction pathways that mediate cell growth, cell polarity, differentiation, and survival[10,11]. However, PTK7 may participate as a co-receptor and its protection by type 1 membrane metalloprotease is implicated in the progression of cancer[12,13]. PTK7 has also been shown to be a key regulator in the Wnt / β-Catenin or Wnt / planar cell polarity pathway, and correlates with aggressive clinicopathological characteristics in cancer[14,15]. Likewise, this receptor is overexpressed in different types of leukemia, colon, lung, prostate, breast, gastric tumors, and even metastases[16–22]. Furthermore, it participates in the migration and endothelial invasion of tumor cells[23–25].

Through imaging, it is possible to identify the expression of tumor biomarkers, using molecular imaging, a non-invasive technique that manages to evaluate the strategies for *in vivo* administration of the tumor target[26,27]. Molecular imaging consists of *in vivo* visualization, characterization and measurement of biological processes at the cellular or molecular level[27,28]. Molecular imaging is a very useful tool for diagnosing cancer. The use of probes that have optimal imaging characteristics provides clinically

essential information for this disease, which would allow a correct selection of the treatment to be followed and the monitoring of its effects[29].

In addition, aptamers have been used as a component of molecular imaging probes since they have the ability to bind, through non-binding covalent bonds, with high affinity and specificity for a molecular target[30,31]. They are oligonucleotides (ssDNAs or RNAs) that have a three-dimensional structure characterized by loops, stems or hairpins. Physicochemical properties, such as temperature and pH stability give an advantages to be functionalized, compared to antibodies[32,33]. In addition, their chemical synthetic process allows a low cost production and no batch to batch variability[34,35]. Furthermore, aptamers molecular weight (~ 15000Da) and charge provide rapid penetration into target tissues and elimination from the body[31,36]. Also, aptamers not immunogenic and non-toxic effects have been reported. Therefore, the characteristics of aptamers provide great advantages for their use in the development of new molecular imaging agents[37].

Previously, we have modified the Sgc8-c aptamer to generate molecular imaging probes in the diagnosis of cancer[37–40]. The Sgc8-c aptamer is DNA (41 nt) and selectively recognizes the PKT7 receptor with a K_d = 0.78 nM[10,41]. We have developed potential molecular imaging probes in different tumor models, through *in vitro* and *in vivo* evaluation. In this sense, radiolabelled probes (Sgc8-c-NOTA-^{67}Ga, Sgc8-c-DOTA-^{67}Ga, Sgc8-c-HYNIC-^{99m}Tc) have been reported to have better tissue penetration and ability to accurately measure tissue, resulting in that allows quantitative images of the whole body to be obtained[37–40]. Likewise, the fluorescent probe (Sgc8-c-Alexa647) allows the generation of optical images in the near infrared region with little interference, achieving optimal contrasts due to the molecules present in the tissues do not exhibit high absorption in that spectral region[37,38]. These features are very useful to perform, for example, guided surgeries in real time42,43. Even, using the appropriate imaging probes, it is possible to identify metastases[44]. Likewise, the sensitive and effective detection of PTK7 may represent a good strategy in the early diagnosis of melanoma. Due to this, the present work evaluates the potential of Sgc8-c probes in two different melanoma models, one being metastatic, in order to optimize biological control methods, both biodistribution and imaging.

Results And Discussion

PTK7 expression in B16F10 cells. Firstly, we evaluated the presence of PTK7 in metastatic melanoma B16F10 cells by flow cytometry and western blot. Previously, was evaluated in non-metastatic B16F1 melanoma cells[37]. Flow cytometry assays performed with a commercial anti-PTK7 antibody as probed reveled that approximately 40 % of the B16F10 cells expressed detectable levels of PTK7. Of note, near to 80 % of the positive control CCRF-CEM cells stained for PTK7, while the negative control, U87MG cells, showed null signal (Fig. 1A). Additionally, the Western blot studies confirmed the presence of PTK7 receptor on B16F10 cells (Fig. 1B, full-length gels are shown in Figure S1 in Supporting Information).

In vitro binding studies. Two different strategies were employed to analyze the ability of Sgc8-c probes to interact to B16F10: the use of the radiolabelled probe (Sgc8-c-NOTA-^{67}Ga) that can be measured by gamma counter system, and the use of the fluorescent-probe (Sgc8-c-Alexa647), which allows analysis by flow cytometry and western blot.

The results showed that the Sgc8-c-NOTA-^{67}Ga probe binds to the B16F10 cell line. It was found that the binding percentage increased with time with significant differences at 4 h of incubation (Fig. 2). Regarding the blocking test of cells with the unlabeled aptamer, it was observed that the percentage of binding to the labeled probe decreases (compare 2 h of incubation and blocking incubation, $p < 0.05$, Fig. 2) indicating that there was a competition between both compounds confirming the probe interaction with PTK7.

For fluorescent-flow cytometry assays, melanoma B16F10 cells were incubated with different concentrations of Sgc8-c-Alexa647. Figure 3 shows the percentage of positive cells and the specific mean fluorescence index (MFI). Results showed that the percentage of PTK7 positive cells is dependent on probe concentration, reaching a maximum of 80 % of B16F10 cells with approximately 0.5 μM. Likewise, the MFI indicates the amount of the probe that binds to PTK7, more precisely, the abundance of proteins at individual population cell level[45]. This suggests that the B16F10 cell line expresses significant high levels of the PTK7 receptor (Fig. 3).

According to cytometry analysis, saturation concentration was reached at 0.3 μM of apatmer without achieving 100 % of the B16F10 cells. This phenomenon could be explained by different cell division and diferentiation stage in cell culture. In addition, a molecular cleavage phenomenon has been described upon Sgc8-PTK7 interaction[46]. If the cleaved PTK7 receptor had been excreted into the supernatant of the medium, as result of cleavage mechanism of the aptamer-PTK7 complex, it would be the cause of not reaching saturation when the process was analyzed by flow cytometry. Then, if the cleaved PTK7 receptor is excreted into the supernatant of the medium, as result of cleavage mechanism of the aptamer-PTK7 complex, its detection by flow cytometry is not possible. However, all experiments were performed in ice so the chances of cleavage are almost null. Besides, Western blot studies using supernatants rejected this hypothesis. The results indicated that both the antibody and the fluorescent probe only recognize proteins from the cell pellet (Fig. 1B) showing that there was no detectable molecular cleavage. Based on these results the hypothesis that the fast complex internalization does not allowing saturation due to the absence of a membrane. For this reason, fluorescent confocal microscopy studies were performed to demonstrate the internalization of the receptor (see below).

In vivo binding studies. Previously to perform the *in vivo* biological studies we analyzed the ability of the Sgc-8-c-Alexa647 probe to recognize *in vivo* the PTK7 presence in target organs. For this, flux cytometry studies were performed on B16F10-tumors, liver, spleen, and bone marrows as negative controls. The results showed that the fluorescent-probe marked high level of tumoral cells while in the rest of the non-target organs the percentage of positive cells were very low (Table 1).

Table 1
Percentage of positive cells for *in vivo* exposed organs to probe Sgc8-c-Alexa647.

Organ / Time (h)	Percentage of positive cells (%, ±SD, n = 5)		
	0.5	2	24
Liver	3.80 ± 2.51	0.70 ± 0.35	0.30 ± 0.17
Spleen	1.10 ± 0.40	2.20 ± 1.15	0.60 ± 0.15
Bone marrow	0.93 ± 0.25	1.40 ± 0.49	0.60 ± 0.21
B16F10 tumor	86.40 ± 3.67	81.20 ± 4.55	82.80 ± 5.84

Confocal microscopy. Another mechanism propose for Sgc8-PTK7 interaction is complex internalization[47]. For this reason, fluorescent confocal microscopy studies were performed to demonstrate the internalization of the receptor on the studied tumoral cells. To perform confocal microscopy assays, the B16F10 tumor cells were incubated with the Sgc8-c-Alexa647 probe during different times. The nuclei were marked with the Hoechst marker and the membrane with WGA-green. Clearly, since the first time of the study it was evident that the Sgc8-c-Alexa647 probe was internalized by the cells (Fig. 4).

Once it was observed that Sgc8-c-Alexa647 is internalized, it was analyzed if the probe was also co-localized within the endosomes like other aptamers-probes[47,48]. For that, tumor cells were incubated with the fluorescent probe for different times and subsequently analyzed the early endosomes with *Rab5* and the nuclei with *Hoechst*. Sgc8-c-Alexa647 was observed to co-localize within endosomes in all cell lines (Fig. 5 and Figure S2 in Supporting Information). Similarly, it was observed that the signal from the probe shows a tendency towards polarization. It has been seen that PTK7 is not found homogeneously distributed uniformly in the cell membrane, presenting a dynamic role in cell polarization[49].

In vivo biological studies. *In vivo* studies using both Sgc8-c-Alexa647 and Sgc8-c-NOTA-^{67}Ga probes have been performed in murine melanoma models. To do this, once the induced tumors were palpable, probes were i.v. administered and imaging and biodistribution studies were performed at different times after injection. The results showed interesting characteristics regarding the uptake of the probes in the tumor (Fig. 6, and Figures S2 and S3 in Supporting Information). Rapid tissue penetration was visualized, with tumor retention (Fig. 6 and Figure S3 in Supporting Information). Using the fluorescent probe, a tumor uptake of 32.9 % was observed at 2 h post-injection (pi), increasing significantly at 24 h (42.4 %) and at 48 h (50.3 %).

The radiolabeled probe showed the same tendency as the fluorescent probe to increase tumor uptake over time. At 2 h pi, a tumor uptake of 8.4 %ID/g was observed, increasing significantly at 24 h (28.8 %ID/g). Then, at 72 hours pi, tumor uptake decreased slightly (17.6 % ID/g), a non-significant signal comes from other organs, which allows us to observe a clear signal from the tumor for that time (Figs. 6, 9 and S3 in Supporting Information). Urinary elimination was observed, for both probes, at early time

points. At 0.5 h after the injection of the fluorescent probe, 3.2 % was eliminated, increasing to 42.5 % at 2 h pi (Fig. 6 and Figure S3 in the Supporting Information) and at 0.5 h 7.1% ID was observed for the radioactive probe, which decreased at 2 h to 4.2 %ID (Fig. 6). These data were determined by the renal values that were due to the elimination of the probes or their metabolites (Figs. 6 and 8). However, it was possible to distinguish the high signals from both tumor and liver in the *in vivo* and ex vivo images, which were higher in the tumor at later time points (Figs. 8 and 9). *In vivo* blocking studies with Sgc8-c-NH_2 showed a statistically significant decrease of tumor signal for the fluorescent probe (Fig. 6 and Figure S3, Supporting information), confirming specific probe training.

Differences in signal values between organs and tumor were evident in both tumoral models and with both probes, resulting in an optimal tumor/non-tumor organ ratio, having a significant increase over time (Fig. 7). Mainly at 48 h pi with radiolabeled probe in the metastatic model, generated by B16F10 cells, showed a tumor / muscle ratio of 35.5 (Fig. 7B and Figure S4 for B16F1 model in Supporting Information). Likewise, it was observed that tumor uptake increased significantly with the time of post-injection in both models (Figure S5 in Supporting Information). However, it was observed that the tumor uptake was slightly higher in the metastatic melanoma model, generated with the B16F10 cell line, than with the B16F1 non-metastatic melanoma model (Fig. 6 and Figure S5 in Supporting Information). This difference could be explained by an increase in the expression of PTK7, since it has been seen that in metastatic melanomas, this receptor is one of the tyrosine kinases that participates in the positive regulation of the formation and function of the invadopodia[9]. Also, this difference in the distribution of the probes, which is also observed in the images obtained by confocal microscopy, could be affected by a structural heterogeneity in the tumor vasculature, since it has been seen that the models generated with the B16F10 line show a significant improvement in vascular density[50].

Conclusions

The interesting results described herein together our previous studies[37,40], showed that both probes developed with the Sgc8-c aptamer are potential tools for their specific use in the early detection of melanoma. The results of *in vitro* studies were consistent with those obtained for biodistributions and the *in vivo* imaging. Obtained interesting characteristics related to the uptake of the probes in the tumor, with optimal tumor/non-target organs ratios. Even these methodologies applied here allowed us to detect differences in the expression of the tumor marker PTK7 in two different types of melanomas. However, it should be studied in depth whether this difference in the expression of PTK7 is really involved in signaling pathways that, consequently, grant greater metastatic power to cells.

The optimal tumor uptakes of the probes, in this new model of metastatic melanoma, make them promising tools to facilitate *in vivo* diagnosis and thus select an appropriate therapy. These probes could also be advantageous for developing intraoperative imaging devices, combined or not, the properties of both probes for use in guided surgeries; identifying and pointing out the tumor margins, helping in the surgical resection of tumors and even helpful in detecting metastases[42,51]. A deepened study with the

metastatic melanoma model are currently in progress with the aim to improve the use of probes in early diagnosis that allows the selection of an efficient and personalized therapy, and even for monitoring after remission.

Our results support the potential role of the Sgc8-c-NOTA-^{67}Ga and Sgc8-c-Alexa647 as molecular imaging probes optimum to improve strategies in non-invasive molecular diagnosis in melanoma, as well as theranostic aproaches.

Methods

Synthesis and purification of Sgc8-c-NOTA-67Ga and Sgc8-c-ALEXA-647. The synthesis and purification of both probes were performed following previous reports from our laboratory[37,39,40].

In vitro biological studies

Tumor cell lines.*Mus musculus* melanoma B16F1 (ATCC, CRL-6323), *Mus musculus* metastatic melanoma B16F10 (ATCC, CRL-6475) and *Homo sapiens* glioblastoma U87 MG (ATCC, HTB-14) cell lines were grown in adherence in Dulbecco's Modified Eagle's Medium (DMEM) (Capricorn, Ebsdorfergrund, Germany) supplemented with 10 % fetal bovine serum (FBS, Sigma-Aldrich, St. Louis, USA) and 2 mM L-glutamine (Sigma-Aldrich, St Louis, USA). *Homo sapiens*, acute lymphoblastic leukaemia CCRF-CEM (ATCC, CCL-119) cell line was grown in a suspension of RPMI-1640 medium (Sigma-Aldrich, St. Louis, USA) supplemented with 10 % FBS and 2 mM L-glutamine. The CCRF-CEM and U87 MG cell lines were used as a positive and negative controls, respectively[52,53]. All cell lines were provided from ATCC (American Type Culture Collection, VA, USA) and were cultured at 37°C with 5 % CO_2.

Binding studies for radio-probe. For *in vitro* cell binding assays, 1.0×10^6 cells from the B16F10 cell line were washed with sterile Phosphate-buffered saline (PBS) pH 7.4, centrifuged at 1000 rpm for 3 min and incubated with 100000 cpm of the Sgc8-c-NOTA-^{67}Ga probe by 0.5, 2 and 4 h at 37°C. In addition, a competition assay was performed by incubating cells with an excess of underivatized aptamer (Sgc8-c-NH_2, 5 µg, 0.4 nmol) for 0.5 h a 37°C. After 0.5 h, these same cells were incubated with the labeled probe for an additional 2 h at 37°C. At the end of the incubation time, the medium was removed and the cells were resuspended and washed twice with PBS, centrifuging at 1000 rpm for 3 min. The test was done in quintupled. The activity retained in the cells was measured on a gamma counter (PC-RIA MAS, Stratec).

Binding studies for fluorescent-probe. The murine tumor cell line B16F10, and the human tumor cell lines CCRF-CEM and U87 MG, were washed with sterile PBS pH 7.4, centrifuged at 1000 rpm for 3 min and approximately, 5×10^5 cells were incubated at 37°C for 30 min with different concentrations of the Sgc8-c-Alexa647 probe (0.007, 0.3 and 1 µM). After incubation, the medium was removed by centrifugation at 1000 rpm for 3 min and washed with PBS, and centrifuging again at 1000 rpm for 3 min. The test was done in quintupled. For each sample, 10000 events were detected using a 635nm excitation, laser detector and BP 660 / 20 nm. The FACS Canto II flow cytometer (BD Biosciences, San Diego, CA, USA)

equipment and data were analyzed using FACS Diva and FlowJo software. These results were validated with an anti-PTK7-PE antibody (United States Biological. Clone Type: Polyclonal. Catalog Number: 033359-PE). Specific mean fluorescence indices (MFIs) were calculated as the mean fluorescence of Sgc8-c-Alexa647 cells positive in the presence of aptamer over the mean fluorescence of the entire cell population in the absence of aptamer.

Western blotting. Supernatants and cell pellets from B16F10 cell cultures were collected separately. Pellets were washed with sterile PBS pH 7.4, centrifuged at 1,000 rpm for 3 min and stored at -20°C until use. Supernatant proteins were obtained by precipitation with trichloroacetic acid (TCA). Briefly, supernatants were centrifuged for 15 min at 4,000 g at 4°C. The supernatants from this centrifugation were recovered and passed through a 0.22 µm filter. Then, TCA (10 % final solution) was added and incubated for 1 h on ice. Pellets were obtained by centrifugation, for 30 min at 13,000 rpm and at 4°C, and further washed three times with 1 mL of acetone and allowed to dry. Finally, proteins were resuspended in 500 µL of PBS pH 7.4. The amount of sample to be used in the Western blot was normalized, quantifying the samples using the bicinchoninic acid assay. Subsequently, these samples were run on a 12 % SDS-PAGE gel at 100 V and the blotting membrane was transferred overnight at 400 mA and at 4°C. The membrane was blocked with 5 % milk in PBS pH 7.4, for 2 h at room temperature (RT). Subsequently, it was incubated with either the Sgc8-c-Alexa647 probe (10µg, 0.8 nmol) or the anti-PTK7-PE antibody, at the concentrations recommended by the manufacturer. Three washes with PBS/TBS were performed before the membrane was observed in an imaging equipment (In-Vivo MS FX PRO instrument, Bruker, Billerica, USA).

Confocal microscopy. To perform confocal microscopy assays, 1×10^5 cells from the B16F10 and B16F1 tumor cell lines were grown on round glass coverslips (12 mm) inside 24-well plates. These cells were incubated with the Sgc8-c-Alexa647 probe (10 µg, 0.8 nmol) for different times (2, 4, and 16 h). Cells were washed with sterile PBS pH 7.4 and fixed with 4 % paraformaldehyde. Subsequently, the coverslips were placed in a humid chamber, the cells were blocked with 2 % bovine serum albumin in PBS for 20 min at RT and then they were blocked for an additional 15 min, also at RT, with the same solution but adding Triton (0.3 %). Cells were incubated for 1 h at RT with the *Hoechst 33342* nuclear marker (1:100, ImmunoChemistry Technologies, LLC) and with the *WGA-green* membrane marker (1:100, thermofisher scientific, USA). They were washed three times with PBS pH 7.4 and three more times with mili Q water. The coverslips were mounted with ProLong® (thermofisher Scientific, USA) and the images were taken in the confocal microscope LEICATCS-SP5-DMI6000 (HeNe laser, 10mW: 633 nm). To determine if the probe was internalized endosomically, we followed the same protocol as before, incubating for 0.5, 2 and 4 h and instead of using a membrane marker, the early endosomal marker *Rab5* (rabbit, 1:100, C8B1 mAb 3547, Cell Signaling Technology, USA) was used. The secondary antibody anti-rabbit IgG, Alexa 488-conjugated (goat, 1:500, ab 150077 Abcam, USA) was used.

In vivo biological studies

Animals. Female C57BL/6 mice, 8 to 12 weeks of age, were used for the *in vivo* evaluation. Animal experimentation protocols were approved by the Ethical Committee of the University for Animal Experimentation, Uruguay (approval number: 240011-001891-17), all experiments were performed following the principles outlined in the Declaration of Helsinki and complying with the ARRIVE guidelines. Animals were purchased from URBE (Unidad de Reactivos y Biomodelos de Experimentación, Facultad de Medicina-Universidad de la República, Montevideo, Uruguay). Animals were housed in wire mesh cages (racks with filtered air) at 20 ± 2 ^{o}C with cycle of 14 hours of light and 10 hours of darkness. They were fed *ad libitum* to standard pellet diet and given water *ad libitum* and were used after a minimum of 3 days acclimation to the housing conditions. Animals were monitored daily, recording their behavior and the presence or absence of tumor. Tumor location and volume was recorded, and checked that they did not exceed a diameter of 5 mm. Isoflurane was used for anesthesia and at the end of the experiments the animals were sacrificed by cervical dislocation.

Binding studies for fluorescent-probe. For this assay 2.5 × 10^5 cells/100 mL of the B16F10 cell line were injected subcutaneously into the right flank of C57BL/6 mice. Once tumors were palpable (10–12 days), the Sgc8-c-Alexa647 probe (25 µg, 2 nmol) was injected intravenously (i.v.) through the tail vein. At 0.5, 2 and 24 h post injection, mice were sacrificed to obtain the tumor, liver, spleen and marrow derived from the femur. Organs and tissues were disaggregated by passing through a cell strainer 70 µm (BD Bioscience) and resuspended in sterile PBS pH 7.4. For each sample, 10000 events were detected using the same laser, detector, and equipment mentioned above. The test was done in quintupled. Data were analyzed using FACS Diva and FlowJo software.

Imaging and biodistribution. To generate the melanoma tumor model, murine cell line B16F10. Tumors were induced in the C57BL/6 mice as described above for B16F10. Once melanomas were palpable, the Sgc8-c-Alexa647 probe (25 µg, 2 nmol) was injected i.v. and at 0.5, 2, 24 and 48 h post- injection (n = 5 per time group), mice were sacrificed. Ex vivo images of organs (liver, heart, lungs, spleen, kidneys, thyroid, muscule, bone, blood and tumor) were taken using the imaging equipment above mentioned, with the X-ray and fluorescence model. This study was compared with the melanoma tumor model generated with B16F1 cells. The results were expressed in ROI and the tumor/blood and tumor/muscle ratios were calculated. A competition test was performed. One group of mice (n = 5) were first i.v. injected with Sgc8-c-NH_2 in excess of 5 times more than the probe. After 30 min post-injection, the same mice were i.v. injected with the Sgc8-c-Alexa647 probe. After 2 h mice were sacrificed, images taken and organs weighed. Similar evaluation was performed for the radiolabelled probe. Sgc8-c-NOTA-67Ga was i.v. injected (~ 1850 kBq) and biodistribution of the probe was following until 72 h post-injection. Over time, the animals were anesthetized with isoflurane to perform the images *in vivo*. Live images were aquired for 0.5, 2, 24, 48 and 72 h after injection by X-rays and gamma modalities in the imaging equipment. For the biodistributions animals were sacrificed, images were acquired and the levels of radioactivity in the tissue were measured using a gamma counter (PC-RIA MAS, Stratec). Radioactivity levels were expressed as percentage of injected dose per organ gram (%ID/g) and injected dose (%ID). Blocking assays were

also performed, injecting mice first with 0.5 nmol of Sgc8-c-NH_2 and after 30 min re-injected with Sgc8-c-NOTA-67Ga and at 2 h the imaging and biodistribution studies were performed.

Statistical analysis. Statistical analysis was performed using the Student's t-test and the *p* values of significance indicated in each figure.

Declarations

Competing interests

The authors declare no competing interests.

Acknowledgements

The authors specially thank BSc. Camila Davison (Uruguay) for her collaboration in the confocal microscopy analysis. We are grateful Agencia Nacional de Investigación e Innovación (Uruguay) for E.S. scholarship (POS_NAC_2017_1_140364).

Author contributions

M.M, V.C. and H.C. conceived all the experiments; E.S. conducted all the experiments; M.F. contributed in the animal experiments; A.M. contributed in the confocal microscopy experiments. All authors reviewed the manuscript.

References

1. Garbe, C. & Leiter, U. Epidemiology of melanoma and nonmelanoma skin cancer-the role of sunlight. *Adv. Exp. Med. Biol.* **624**, 89–103 (2008).
2. Carr, S., Smith, C. & Wernberg, J. Epidemiology and risk factors of melanoma. *Surg. Clin. North Am.* **100**, 1–12 (2020).
3. Schadendorf, D., Fishe´pr, D. E, Garbe, C., Gershenwald, J. F., Grob, J. J., Halpern, A., Herlyn, M., Marchetti, M. A., McArthur, G., Ribas, A., Roesch, A. & Hauschild, A. Melanoma. *Nat. Rev. Dis. Prim.* **1**, 1–20 (2015).
4. Marsden, J. R., Newton-Bishop, J. A., Burrows, L., Cook, M., Corrie, P. G., Cox, N. H., Gore, M. E., Lorigan, P., Mackie, R., Nathan, P., Peach, H., Powell, B. & Walker, C. Revised UK guidelines for the management of cutaneous melanoma. *J. Plast. Reconstr. Aesthetic Surg.* **63**, 1401–1419 (2010).
5. Abbas, O., Miller, D. D. & Bhawan, J. Cutaneous malignant melanoma: Update on diagnostic and prognostic biomarkers. *Am. J. Dermatopathol.* **36**, 363–379 (2014).
6. Ohsie, S. J., Sarantopoulos, G. P., Cochran, A. J. & Binder, S. W. Immunohistochemical characteristics of melanoma. *J. Cutan. Pathol.* **35**, 433–444 (2008).

7. Eisenstein, A., Gonzalez, E. C., Raghunathan, R., Xu, X., Wu, M., McLean, E. O., McGee, J., Ryu, B. & Alani, R. M.. Emerging biomarkers in cutaneous melanoma. *Mol. Diagnosis Ther.* **22**, 203–218 (2018).
8. Halaban, R. Signal transduction in normal and malignant melanocytes. *Pigment Cell Res.* **7**, 89–95 (1994).
9. Revach, O.-Y., Sandler, O., Samuels, Y. & Geiger, B. Cross-talk between receptor tyrosine kinases AXL and ERBB3 regulates invadopodia formation in melanoma cells. *Cancer Res.* **79**, 2634–2648 (2019).
10. Kroiher, M., Miller, M. A. & Steele, R. E. Deceiving appearances: signaling by 'dead' and 'fractured' receptor protein-tyrosine kinases. *Bioessays* **23**, 69–76 (2001).
11. van der Geer, P., Hunter, T. & Lindberg, R. A. Receptor protein-tyrosine kinases and their signal transduction pathways. *Annu. Rev. Cell Biol.* **10**, 251–337 (1994).
12. Lhoumeau, A. C., Puppo, F., Prébet, T., Kodjabachian, L. & Borg, J. P. PTK7: A cell polarity receptor with multiple facets. *Cell Cycle* **10**, 1233–1236 (2011).
13. Golubkov, V. S., Prigozhina, N. L., Zhang, Y., Stoletov, K., Lewis, J. D., Schwartz, P. E., Hoffman, R. M. & Strongin, A. Y. Protein-tyrosine pseudokinase 7 (PTK7) directs cancer cell motility and metastasis. *J. Biol. Chem.* **289**, 24238–24249 (2014).
14. Sun, J. J., Li, H. L., Guo, S. J., Ma, H., Liu, S. J., Liu, D. & Xue, F. X. The increased PTK7 expression is a malignant factor in cervical cancer. *Dis. Markers* **2019**, 1–10 (2019).
15. Yu, B., Wu, K., Wang, X., Zhang, J., Wang, L., Jiang, Y., Zhu, X., Chen, W. & Yan, M. Periostin secreted by cancer-associated fibroblasts promotes cancer stemness in head and neck cancer by activating protein tyrosine kinase 7. *Cell Death Dis.* **9**, 1082 (2018).
16. Kampen, K. R. Membrane proteins: The key players of a cancer cell. *J. Membr. Biol.* **242**, 69–74 (2011).
17. Lin, Y., Zhang, L. H., Wang, X. H., Xing, X. F., Cheng, X. J., Dong, B., Hu, Y., Du, H., Li, Y. A., Zhu, Y. B., Ding, N., Du, Y. X., Li, J. Y. & Ji, J. F. PTK7 as a novel marker for favorable gastric cancer patient survival. *J. Surg. Oncol.* **106**, 880–886 (2012).
18. Endoh, H., Tomida, S., Yatabe, Y., Konishi, H., Osada, H., Tajima, K., Kuwano, H., Takahashi, T. & Mitsudomi, T. Prognostic model of pulmonary adenocarcinoma by expression profiling of eight genes as determined by quantitative real-time reverse transcriptase polymerase chain reaction. *J. Clin. Oncol.* **22**, 811–819 (2004).
19. Zhang, H., Wang, A., Qi, S., Cheng, S., Yao, B. & Xu, Y. Protein tyrosine kinase 7 (PTK7) as a predictor of lymph node metastases and a novel prognostic biomarker in patients with prostate cancer. *Int. J. Mol. Sci.* **15**, 11665–11677 (2014).
20. Gärtner, S., Gunesch, A., Knyazeva, T., Wolf, P., Högel, B., Eiermann, W., Ullrich, A., Knyazev, P. & Ataseven, B. PTK 7 is a transforming gene and prognostic marker for breast cancer and nodal metastasis involvement. *PLoS One* **9**, e84472 (2014).
21. Saha S., Bardelli A., Buckhaults P., Velculescu V. E., Rago C., St Croix B., Romans K. E., Choti M. A., Lengauer C., Kinzler K. W. & Vogelstein B. A phosphatase associated with metastasis of colorectal

cancer. *Science* **294**, 1343–6 (2001).

22. Fazilaty, H. & Mehdipour, P. Genetics of breast cancer bone metastasis: a sequential multistep pattern. *Clin. Exp. Metastasis* **31**, 595–612 (2014).
23. Lu X., Borchers A. G., Jolicoeur C., Rayburn H., Baker J. C. & Tessier-Lavigne M. PTK7/CCK-4 is a novel regulator of planar cell polarity in vertebrates. *Nature* **430**, 93–98 (2004).
24. Shnitsar, I. & Borchers, A. PTK7 recruits dsh to regulate neural crest migration. *Development* **135**, 4015–4024 (2008).
25. Shin, W. S., Maeng, Y. S., Jung, J. W., Min, J. K., Kwon, Y. G. & Lee, S. T. Soluble PTK7 inhibits tube formation, migration, and invasion of endothelial cells and angiogenesis. *Biochem. Biophys. Res. Commun.* **371**, 793–798 (2008).
26. Tong, R., Coyle, V. J., Tang, L., Barger, A. M., Fan, T. M. & Cheng, J. Polylactide nanoparticles containing stably incorporated cyanine dyes for in vitro and in vivo imaging applications. *Microsc. Res. Tech.* **73**, 901–909 (2010).
27. Weissleder, R. & Mahmood, U. Molecular imaging. *Radiology* **219**, 316–333 (2001).
28. Zhuo, Z., Yu, Y., Wang, M., Li, J., Zhang, Z., Liu, J., Wu, X., Lu, A., Zhang, G. & Zhang, B. Recent advances in SELEX technology and aptamer applications in biomedicine. *Int. J. Mol. Sci.* **18**, 1–19 (2017).
29. Murphy, P. S., Patel, N. & McCarthy, T. J. Has molecular imaging delivered to drug development? Philos. *Trans. R. Soc. A Math. Phys. Eng. Sci.* **375**, 20170112 (2017).
30. Breaker, R. R. Natural and engineered nucleic acids as tools to explore biology. *Nature* **432**, 838–845 (2004).
31. Hwang, D. W., Ko, H. Y., Lee, J. H., Kang, H., Ryu, S. H., Song, I. C., Lee, D. S. & Kim, S. A Nucleolin-targeted multimodal nanoparticle imaging probe for tracking cancer cells using an aptamer. *J. Nucl. Med.* **51**, 98–105 (2010).
32. Hicke, B. J., Stephens, A. W., Gould, T., Chang, Y. F., Lynott, C. K., Heil, J., Borkowski, S., Hilger, C. S., Cook, G., Warren, S. & Schmidt, P. G. Tumor targeting by an aptamer. *J. Nucl. Med.* **47**, 668–78 (2006).
33. Famulok, M. & Mayer, G. Aptamers as tools in molecular biology and immunology. *Curr. Top. Microbiol. Immunol*. 123–136 (1999).
34. Ellington, A. D. & Szostak, J. W. *In vitro* selection of RNA molecules that bind specific ligands. *Nature* **346**, 818–822 (1990).
35. Tuerk, C. & Gold, L. Systematic evolution of ligands by exponential enrichment: RNA ligands to bacteriophage T4 DNA polymerase. *Science* **249**, 505–10 (1990).
36. Borbas, K. E., Ferreira, C. S. M., Perkins, A., Bruce, J. I. & Missailidis, S. Design and synthesis of mono- and multimeric targeted radiopharmaceuticals based on novel cyclen ligands coupled to anti-MUC1 aptamers for the diagnostic imaging and targeted radiotherapy of cancer. *Bioconjug. Chem.* **18**, 1205–1212 (2007).

37. Calzada, V., Moreno, M., Newton, J., González, J., Fernández, M., Gambini, J. P., Ibarra, M., Chabalgoity, A., Deutscher, S., Quinn, T., Cabral, P. & Cerecetto, H. Development of new PTK7-targeting aptamer-fluorescent and -radiolabelled probes for evaluation as molecular imaging agents: Lymphoma and melanoma in vivo proof of concept. *Bioorg. Med. Chem.* **25**, 1163–1171 (2017).
38. Calzada, V., Báez, J., Sicco, E., Margenat, J., Fernández, M., Moreno, M., Ibarra, M., Gambini, J., Cabral, P. & Cerecetto, H. Preliminary in vivo characterization of a theranostic aptamer: Sgc8-c-DOTA-67Ga. *Aptamers* **1**, 19–27 (2017).
39. Sicco, E., Báez, J., Margenat, J., García, F., Ibarra, M., Cabral, P., Moreno, M., Cerecetto, H. & Calzada, V. Derivatizations of Sgc8-c aptamer to prepare metallic radiopharmaceuticals as imaging diagnostic agents: Syntheses, isolations, and physicochemical characterizations. *Chem. Biol. Drug Des.* **91**, 747–755 (2018).
40. Sicco, E., Baez, J., Ibarra, M., Fernández, M., Cabral, P., Moreno, M., Cerecetto, H. & Calzada, V. Sgc8-c aptamer as a potential theranostic agent for hemato-oncological malignancies. *Cancer Biother. Radiopharm.* **35**, 262–270 (2020).
41. Shangguan, D., Tang, Z., Mallikaratchy, P., Xiao, Z. & Tan, W. Optimization and modifications of aptamers selected from live cancer cell lines. *ChemBioChem* **8**, 603–606 (2007).
42. Schaafsma, B. E., Verbeek, F. P., Peters, A. A., Van der Vorst, J. R., De Kroon, C. D., Van Poelgeest, M. I., Trimbos, J. B., Van de Velde, C. J., Frangioni, J. V., Vahrmeijer, A. L. & Gaarenstroom, K. N. Near-infrared fluorescence sentinel lymph node biopsy in vulvar cancer: a randomised comparison of lymphatic tracers. *BJOG An Int. J. Obstet. Gynaecol.* **120**, 758–764 (2013).
43. KleinJan, G. H., Hellingman, D., Van den Berg, N. S., Van Oosterom, M. N., Hendricksen, K., Horenblas, S., Valdes Olmos, R. A. & van Leeuwen, F. W. Hybrid surgical guidance: Does hardware integration of γ- and fluorescence imaging modalities make sense? *J. Nucl. Med.* **58**, 646–650 (2017).
44. Liberale, G., Bourgeois, P., Larsimont, D. & Moreau, M. Indocyanine green fluorescence-guided surgery after IV injection in metastatic colorectal cancer: A systematic review. *Eur. J. Surg. Oncol.* **43**, 1656–1667 (2017).
45. Mous, K., Jennes, W., De Roo, A., Pintelon, I., Kestens, L. & Van Ostade, X. Intracellular detection of differential APOBEC3G, TRIM5alpha, and LEDGF/p75 protein expression in peripheral blood by flow cytometry. *J. Immunol. Methods* **372**, 52–64 (2011).
46. Na, H., Shin, W., Ludwig, A. & Lee, S. The cytosolic domain of protein-tyrosine kinase 7 (PTK7), generated from sequential cleavage by a disintegrin and metalloprotease 17 (ADAM17) and γ-secretase, enhances cell proliferation and migration in colon cancer cells. *J. Biol. Chem.* **287**, 25001–25009 (2012).
47. Xiao, Z., Shangguan, D., Cao, Z., Fang, X. & Tan, W. Cell-specific internalization study of an aptamer from whole cell selection. *Chem. - A Eur. J.* **14**, 1769–1775 (2008).
48. Porciani, D., Cardwell L. N., Tawiah K. D., Alam K. K., Lange M. J., Daniels M. A. & Burke D. H. Modular cell-internalizing aptamer nanostructure enables targeted delivery of large functional RNAs in cancer cell lines. *Nat. Commun.* **9**, 2283 (2018).

49. Berger, H., Breuer, M., Peradziryi, H., Podleschny, M., Jacob, R. & Borchers, A. PTK7 localization and protein stability is affected by canonical Wnt ligands. *J. Cell Sci.* **130**, 1890–1903 (2017).
50. Pautu, V., Mellinger, A., Resnier, P., Lepeltier, E., Martin, L., Boussemart, L., Letournel, F., Passirani, C. & Clere, N. Melanoma tumour vasculature heterogeneity: from mice models to human. *J. Cancer Res. Clin. Oncol.* **145**, 589–597 (2019).
51. Liu, Y., Bauer, A. Q., Akers, W. J., Sudlow, G., Liang, K., Shen, D., Berezin, M. Y., Culver, J. P. & Achilefu, S. Hands-free, wireless goggles for near-infrared fluorescence and real-time image-guided surgery. *Surgery* **149**, 689–698 (2011).
52. Yin, J., He, X., Wang, K., Xu, F., Shangguan, J., He, D. & Shi, H. Label-free and turn-on aptamer strategy for cancer cells detection based on a DNA–silver nanocluster fluorescence upon recognition-induced hybridization. *Anal. Chem.* **85**, 12011–12019 (2013).
53. Jacobson, O., Weiss, I. D., Wang, L., Wang, Z., Yang, X., Dewhurst, A., Ma, Y., Zhu, G., Niu, G., Kiesewetter, D. O., Vasdev, N., Liang, S. H. & Chen, X. ^{18}F-labeled single-stranded DNA aptamer for PET imaging of protein tyrosine kinase-7 expression. *J. Nucl. Med.* **56**, 1780–1785 (2015).

Figures

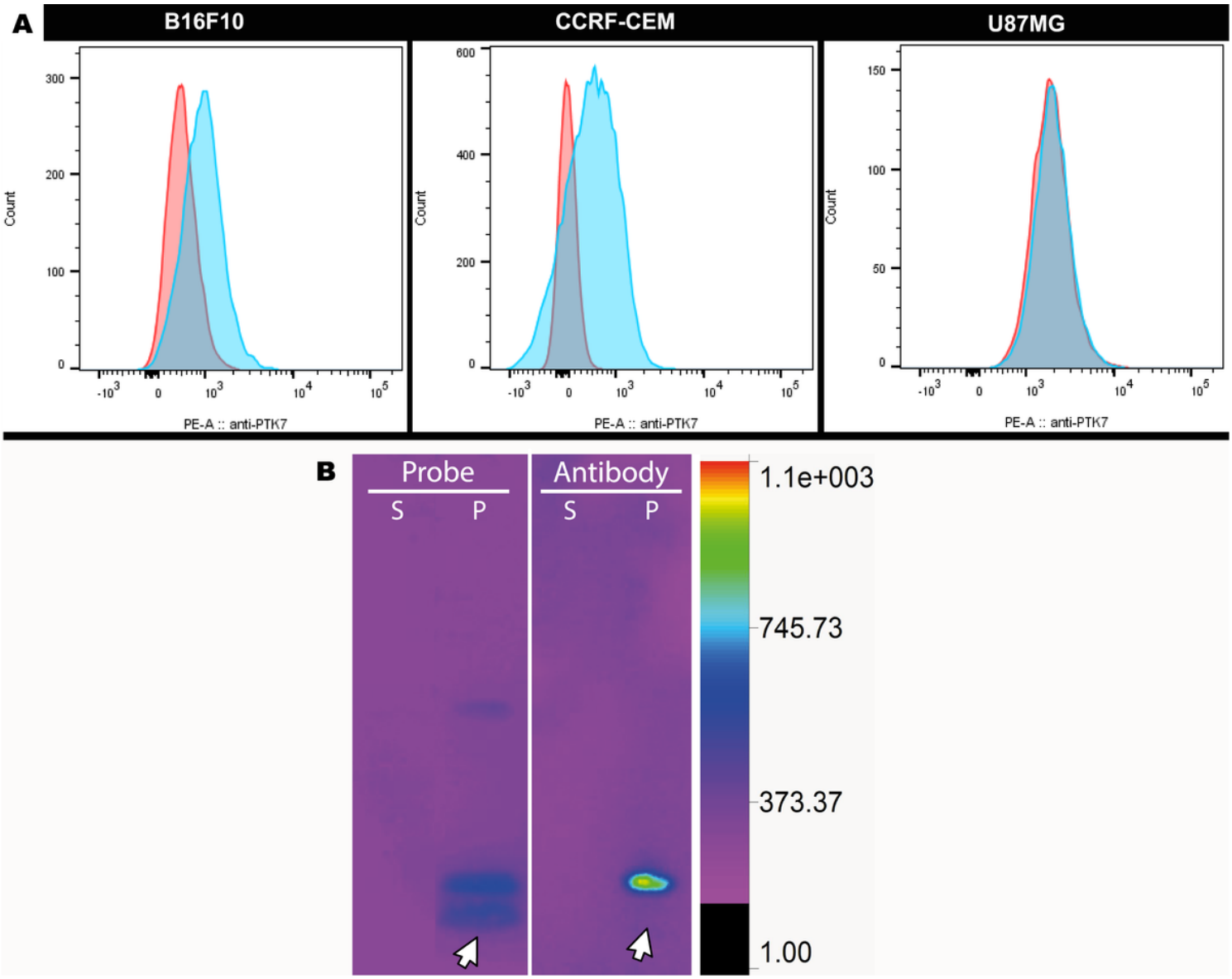

Figure 1

A. Flow cytometry with cell lines B16F10, CCRF-CEM and U87MG. Histograms of cell lines after for incubation with anti-PTK7-PE antibody (in blue) and control (in red). B. Grouping of western blot cropped of proteins extracted from the supernatant (S) and pellet (P) of B16F10 cells culture. Incubation was performed with the Sgc8-c-Alexa647 probe (Probe) and with the anti-PTK7-PE antibody (Antibody). Arrow indicates the presence of PTK7 only in the cell pellet. White dividing line indicates different gels and exposures (full-length gels are shown in Figure S1 in Supporting Information).

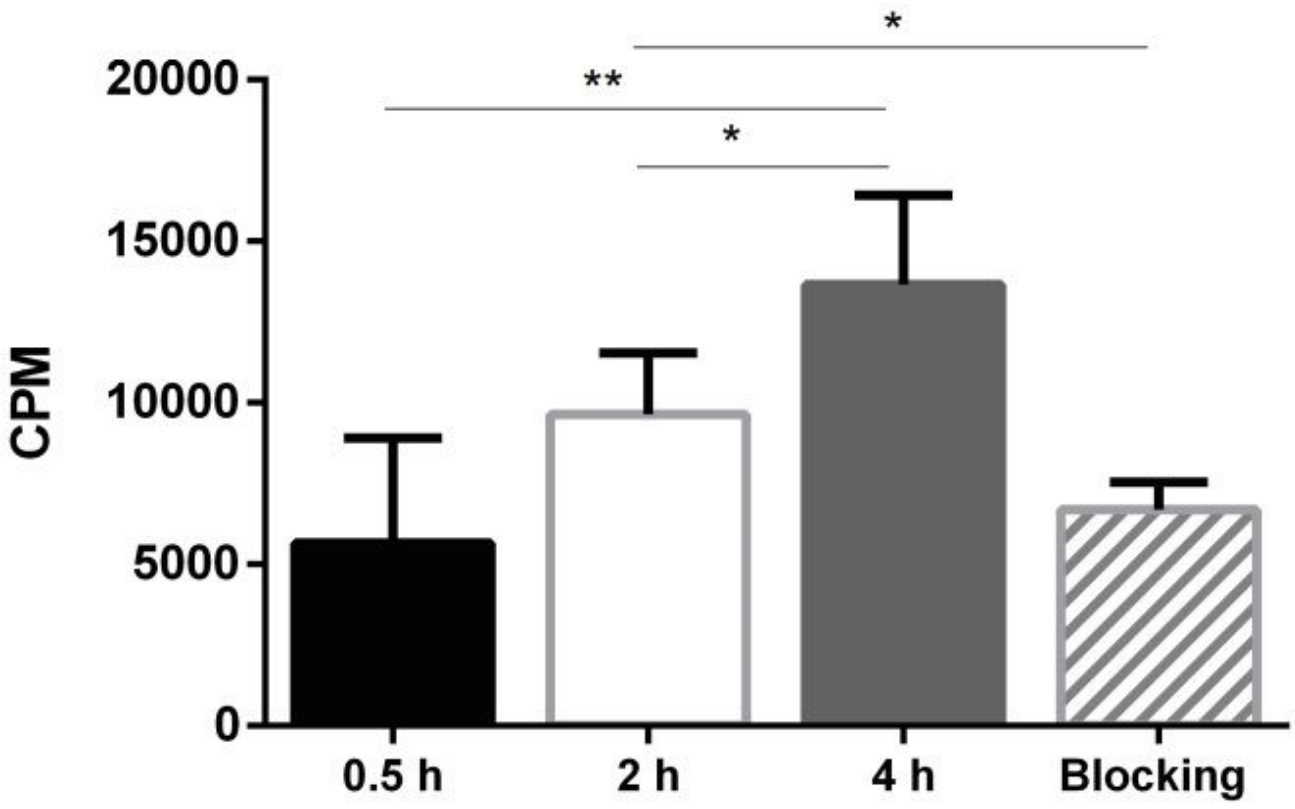

Figure 2

Binding assay with Sgc8-c-NOTA-67Ga in the B16F10 cell line. The probe was incubated for 0.5, 2 and 4 h. Blocking: represents the competition test performed by incubating the cells with an excess of unlabeled aptamer (Sgc8-c-NH2). ** $p < 0.01$, * $p < 0.05$ (Student's t-test).

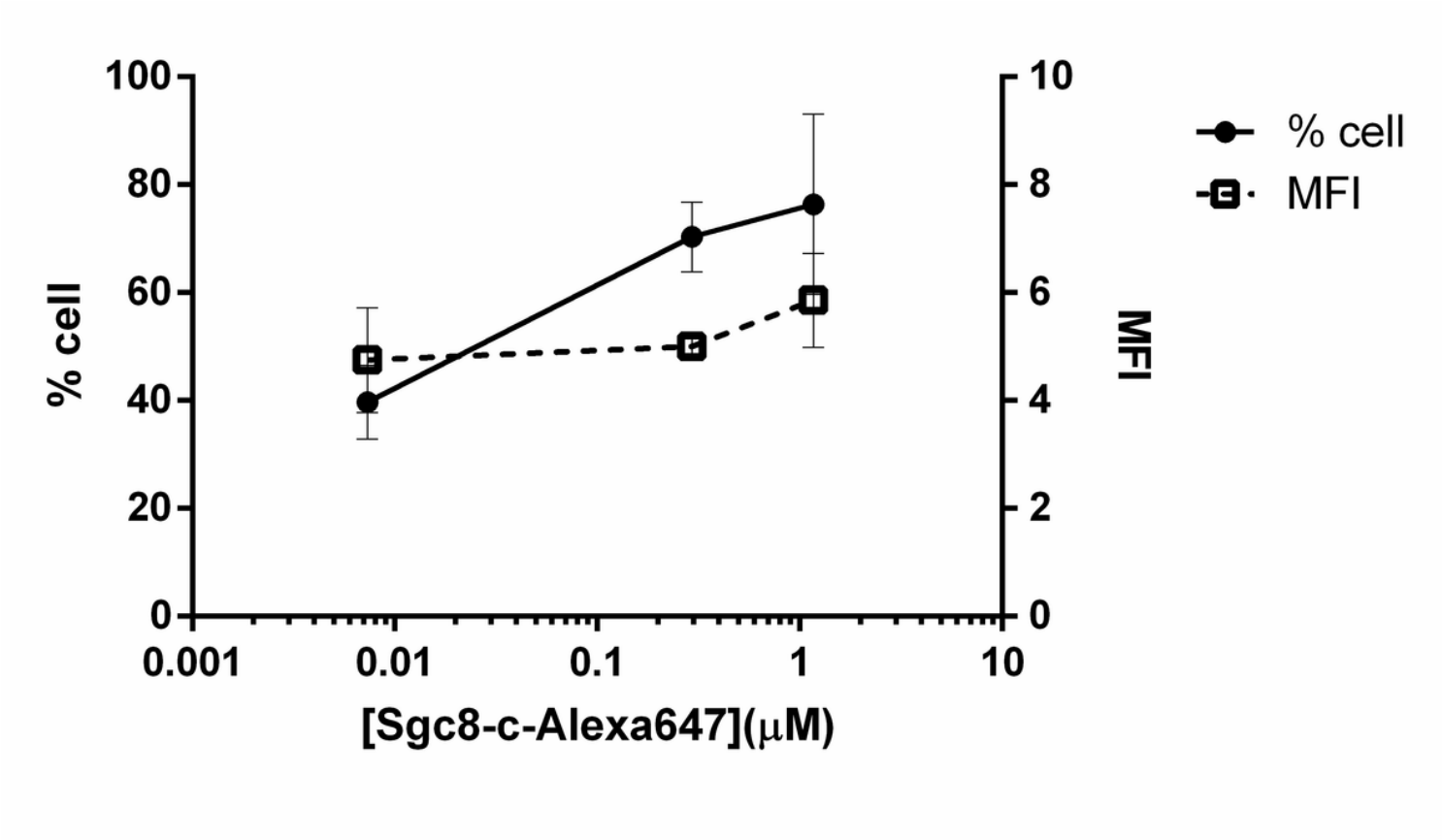

Figure 3

Flow cytometry of B16F10 cell line treated with Sgc8-c-Alexa647. Percentage of positive cells and specific MFI after incubation with the fluorescent probe.

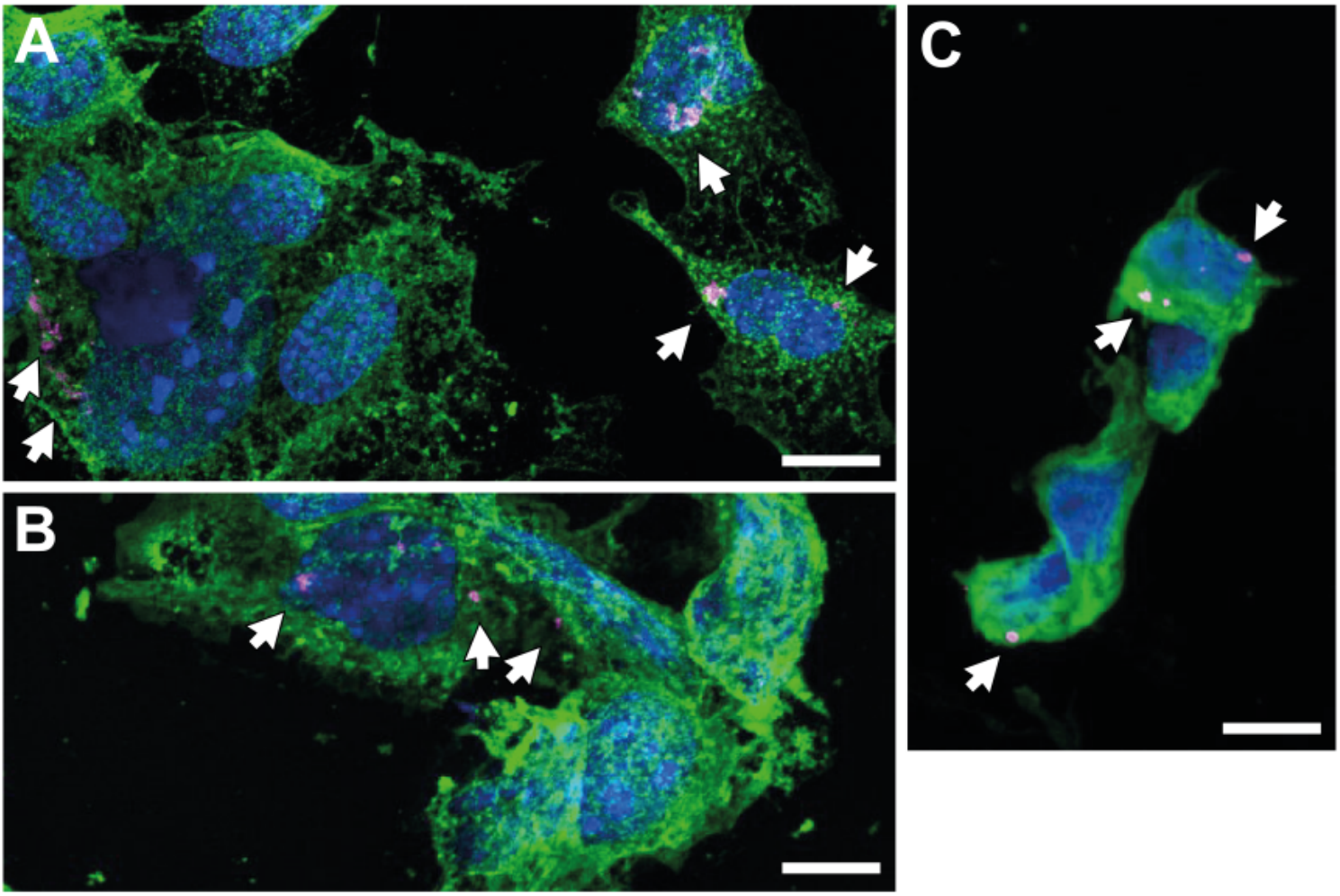

Figure 4

Confocal microscopy of B16F10 tumor cells incubated with fluorescent probe Sgc8-c-Alexa647. In A. are shown cells that were incubated for 2 h with the probe, in B. cells incubated for 4 h and in C. incubated for 16 h. Magenta: Sgc8-c-Alexa647 (white arrows), Blue: Hoechst and Green: WGA-green. Scale bar: 10 μm.

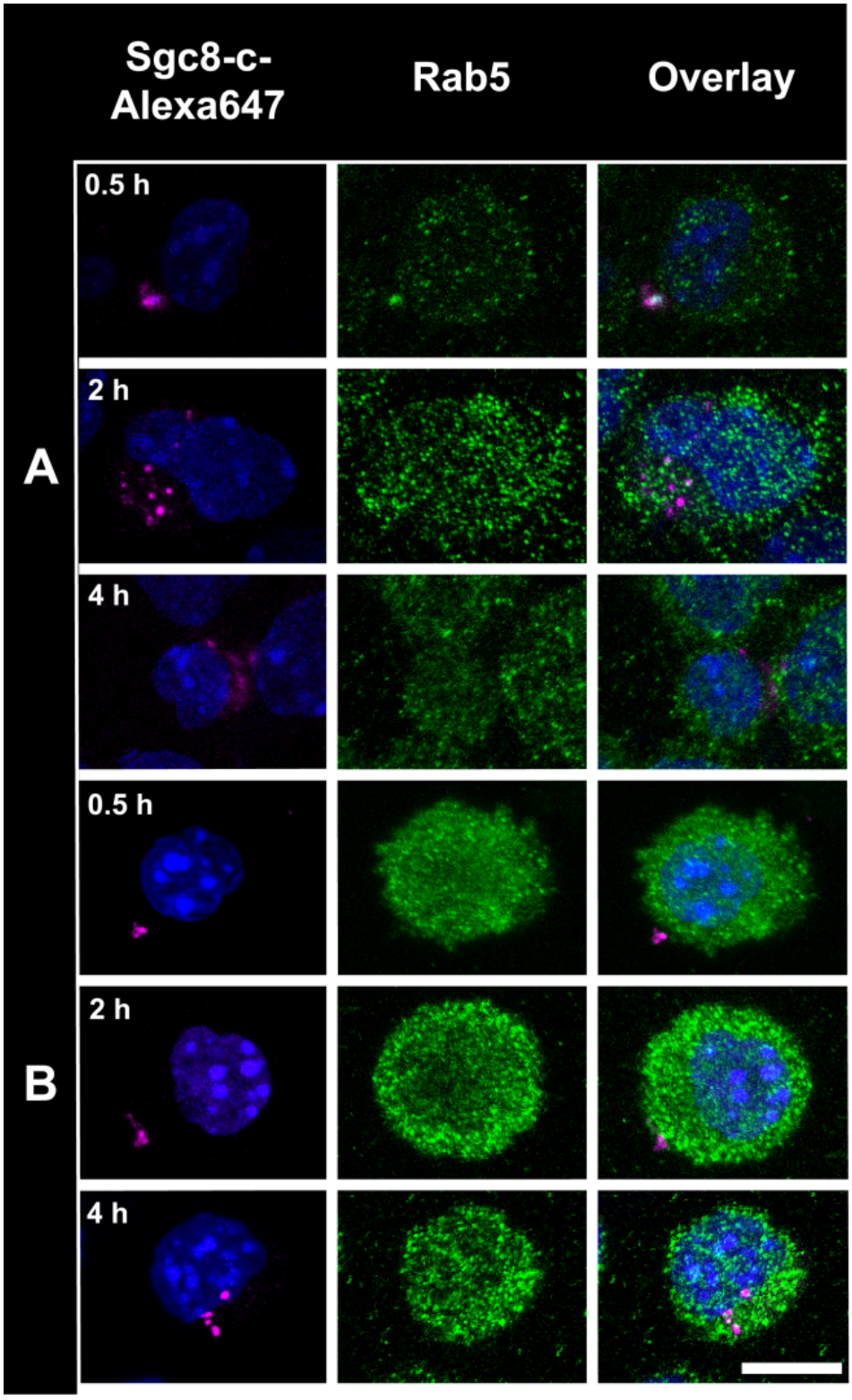

Figure 5

Sgc8-c-Alexa647 co-localize within endosomes. Confocal microscopy of A. B16F10 and B. B16F1 tumor cells incubated for 0.5, 2 and 4 h with the probe. Magenta: Sgc8-c-Alexa647, Blue: Hoechst and Green: Rab5. Scale bar: 10 μm.

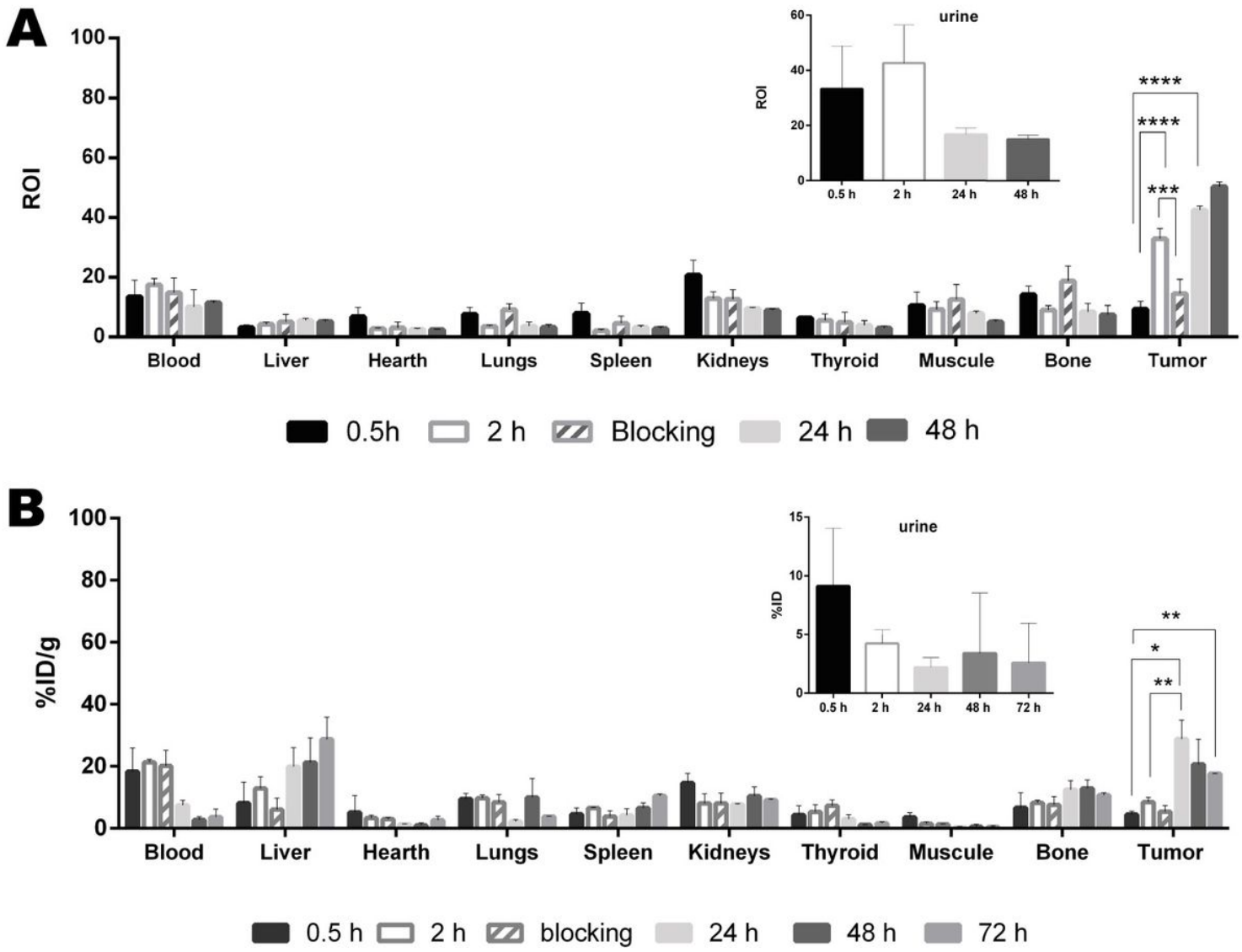

Figure 6

Biodistribution of the probes in B16F10 tumors. A. Biodistribution of Sgc8-cAlexa647 and B. Sgc8-c-NOTA-67Ga. **** $p < 0.0001$, *** $p < 0.001$, ** $p < 0.01$, * $p < 0.05$ (Student's t-test).

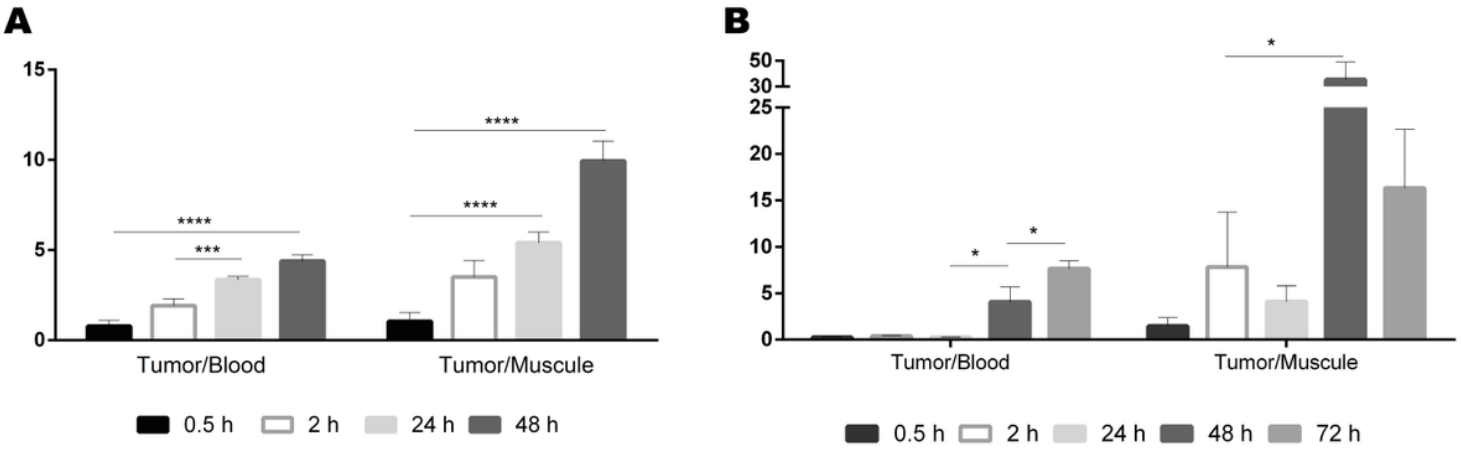

Figure 7

Tumor/blood and tumor/muscle ratios in the tumor model generated with B16F10 cells. A. Sgc8-cAlexa647 and B. Sgc8-c-NOTA-67Ga in the tumor model generated with B16F10 cells. **** $p < 0.0001$, *** $p < 0.001$, * $p < 0.05$ (Student's t-test).

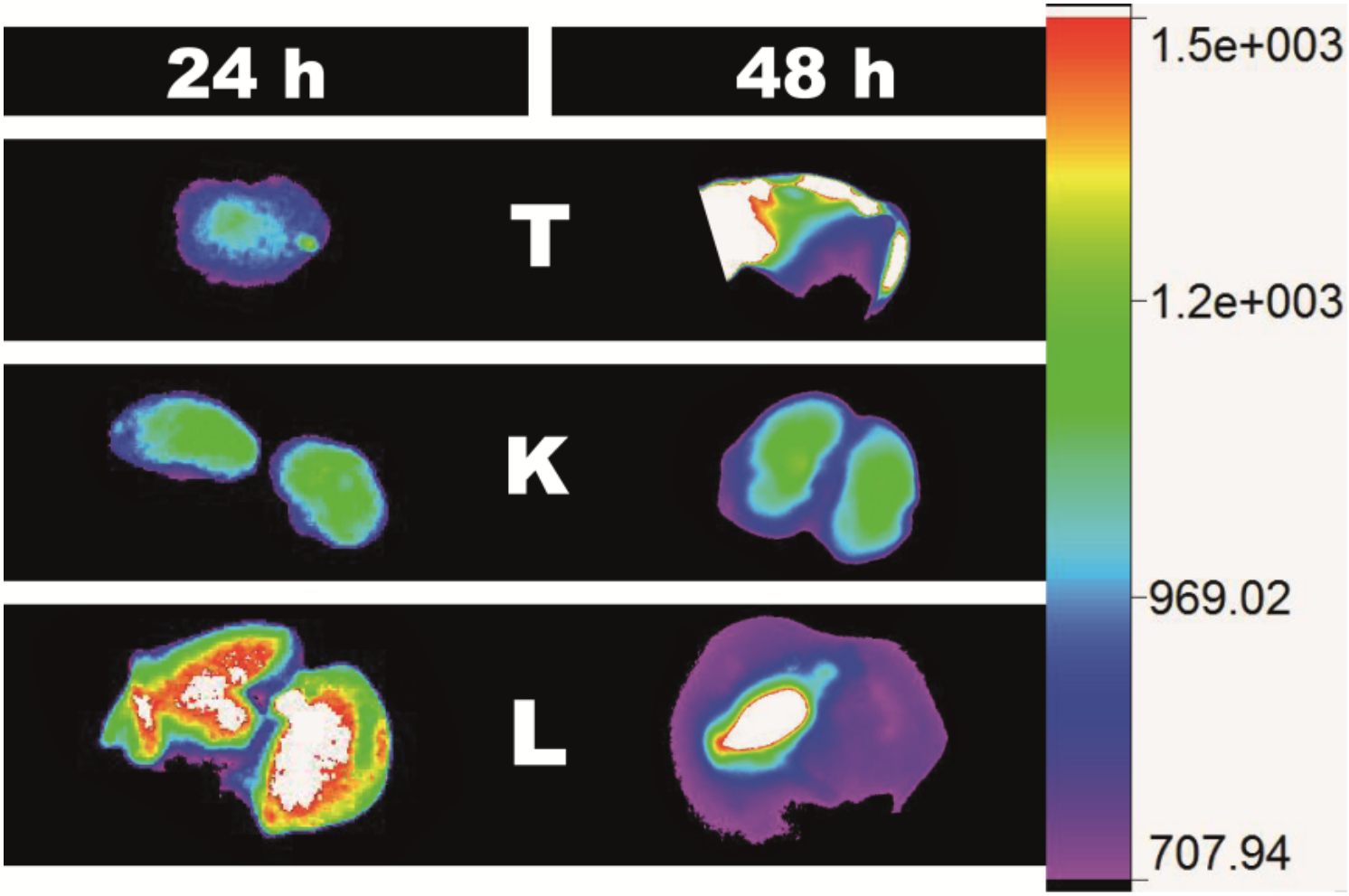

Figure 8

Ex vivo images with Sgc8-c-Alexa647 probe. Tumor (T), kidneys (K) and liver (L) were observed for melanoma tumor model generated with B16F10 cells 24 and 48 hours post-injection of the probe.

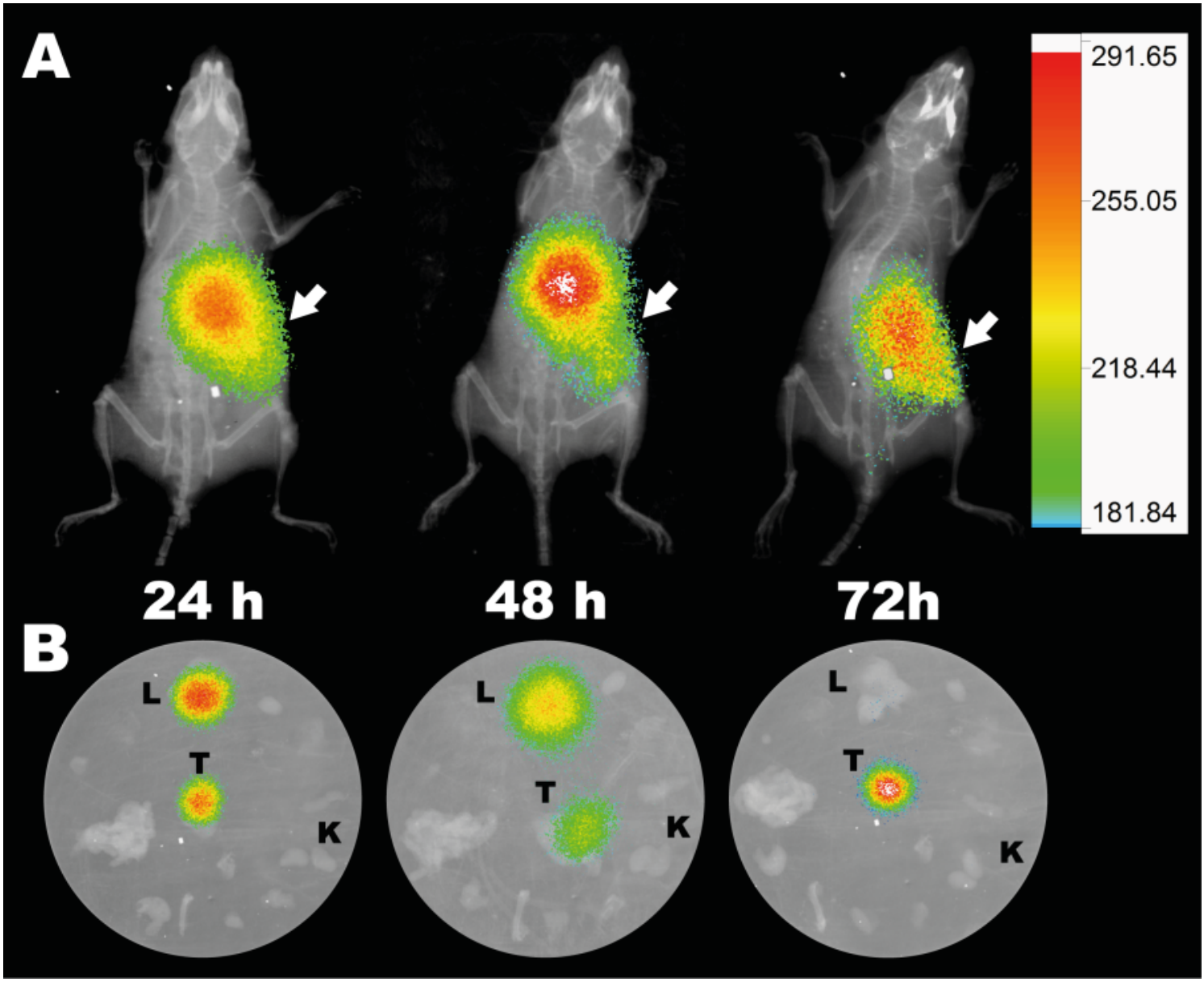

Figure 9

Multimodal images of animals injected with Sgc8-c-NOTA-67Ga probe. A. In vivo and B. Ex-vivo images at 24, 48 and 72 hours post-injection of the probe. Arrow indicates the locations of the tumors. T: tumor, L: liver and K: kidneys. Ex-vivo images also include bone, lungs, blood, heart, muscle, intestine, stomach, thyroid, and spleen.

Supplementary Files

This is a list of supplementary files associated with this preprint. Click to download.

- SupInff.pdf